Structural Insights into How the MIDAS Ion Stabilizes Integrin Binding to an RGD Peptide under Force

David Craig,[1,4,5] Mu Gao,[2,5] Klaus Schulten,[2]
and Viola Vogel[1,3,*]
[1]Center of Nanotechnology and
Department of Bioengineering
University of Washington
Seattle, Washington 98195
[2]Beckman Institute and Department of Physics
University of Illinois, Urbana-Champaign
Urbana, Illinois 61801
[3]Department of Materials
Swiss Federal Institute of Technology (ETH)
Zürich 8093
Switzerland
[4]Neurogenomics Division
Translational Genomics Research Institute
Phoenix, Arizona 85004

Summary

Integrin $\alpha_v\beta_3$ binds to extracellular matrix proteins through the tripeptide Arg-Gly-Asp (RGD), forming a shallow crevice rather than a deep binding pocket. A dynamic picture of how the RGD-$\alpha_v\beta_3$ complex resists dissociation by mechanical force is derived here from steered molecular dynamic (SMD) simulations in which the major force peak correlates with the breaking of the contact between Asp[RGD] and the MIDAS ion. SMD predicts that the RGD-$\alpha_v\beta_3$ complex is stabilized from dissociation by a single water molecule tightly coordinated to the divalent MIDAS ion, thereby blocking access of free water molecules to the most critical force-bearing interaction. The MIDAS motif is common to many other proteins that contain the phylogenetically ancient von Willebrand A (vWA) domain. The functional role of single water molecules tightly coordinated to the MIDAS ion might reflect a general strategy for the stabilization of protein-protein adhesion against cell-derived forces through divalent cations.

Introduction

Integrins are large $\alpha\beta$-heterodimeric transmembrane proteins that mechanically couple the contractile cytoskeleton to the extracellular matrix (ECM). Formation of mechanically stable integrin complexes is critical to transduce mechanical forces between the cell and the ECM. Outside-in forces pulling on integrins regulate maturation and composition of the linkages between integrins and the cytoskeleton (Galbraith et al., 2002; Giannone et al., 2003). Vice versa, cell-derived mechanical forces applied to the ECM via integrins are sufficiently high to partially unfold proteins of the ECM (Baneyx et al., 2002). Integrin binding to ECM proteins is frequently mediated by the tripeptide RGD (Arg-Gly-Asp), which is presented as a loop and binds to a shallow

*Correspondence: viola.vogel@mat.ethz.ch
[5]These authors contributed equally to this work

crevice located between the α_v and β_3 subunit of the integrin head (Xiong et al., 2002). Atomic force microscopy (AFM) and optical tweezers show that substantial force is required to detach RGD-containing proteins, such as those found in fibronectin type III modules or in echistastin, from integrins (Lehenkari and Horton, 1999; Li et al., 2003; Thoumine et al., 2000).

Evidently, integrins can form strong noncovalent bonds with RGD-containing proteins, yet it is surprising that such strong bonds are mediated by a small peptide that binds into a shallow crevice rather than into a deep binding pocket. One of the strongest known noncovalent bonds is formed between biotin and streptavidin, where biotin is buried in a 7 Å deep binding pocket (Evans, 2001; Hyre et al., 2002). The advantage of a deep binding pocket is that the noncovalent bonds formed between a receptor and its ligand are well shielded from attacks by water molecules. The importance of stabilizing interactions by shielding critical force-bearing hydrogen bonds from attacks by free water molecules that would otherwise compete for the hydrogen bonding partners is also essential in enhancing the mechanical stability of proteins (Craig et al., 2004; Lu and Schulten, 2000).

In contrast to the deep binding pocket of streptavidin, the crystal structure of integrin $\alpha_v\beta_3$ bound to a cyclic RGD peptide (Arg-Gly-Asp-{D-Phe}-{N-methyl-Val}, or cyclo-RGDfNMeV) revealed that only the Arg and Asp side chains of the RGD peptide are found to be slightly buried within a shallow crevice located between the α and β integrin subunits, and that the remainder of the peptide is exposed to water (Xiong et al., 2002). Furthermore, divalent cations play a critical role in mediating the binding of integrins to RGD peptides. X-ray crystallographic studies provided the structure of the ligand binding portion of integrin $\alpha_v\beta_3$ (Xiong et al., 2001; Xiong et al., 2002) (see Figure 1), consisting of the β propeller domain of α_v (dark blue in all of our figures) and the βA (or I-like) domain and the hybrid domain of β_3 (magenta in all of our figures). A divalent cation at the MIDAS site in the βA domain contacts the Asp of the RGD peptide (Asp[RGD]) (see Figure 2). The MIDAS site is occupied by the divalent ion only in the RGD-liganded state, but no ion is seen in the crystal structure of the unliganded integrin. The situation is different for some other integrins containing an αA domain (or also referred to as the I domain), where both the liganded and unliganded αA domain can capture a divalent ion at MIDAS (Emsley et al., 2000; Shimaoka et al., 2002). In addition to the MIDAS, two other divalent cation sites, termed ADMIDAS (adjacent MIDAS) and LIMBS (ligand-associated metal binding site), were found in the β_3 integrin near the MIDAS. Located 8 Å from the MIDAS, the ADMIDAS can be occupied by either an Mn^{2+} or a Ca^{2+} ion, no matter whether or not the ligand is present (Xiong et al., 2002). The LIMBS, located 6 Å from the MIDAS, acquires an Mn^{2+} ion when the RGD peptide is present, but it does not favor binding a Ca^{2+} ion. Considerable debate currently exists regarding the functional role of the LIMBS and ADMIDAS ions
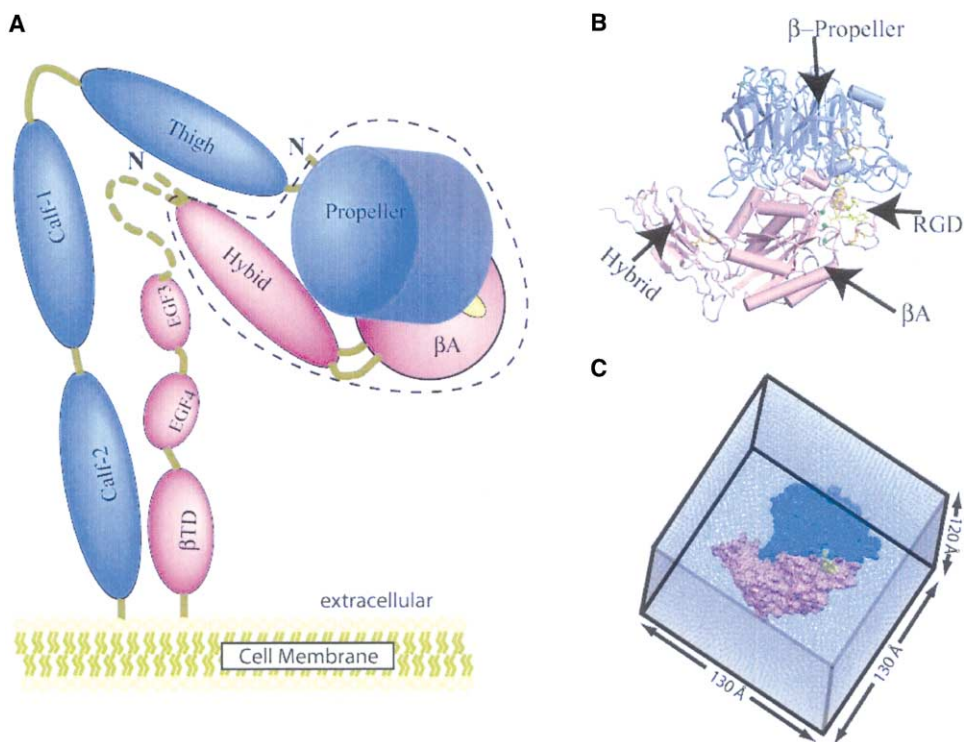
A

B

C

Figure 1. System Setup for the Integrin $\alpha_v\beta_3$ Ligand Complex Simulations

(A) Sketch of the extracellular portion of integrin $\alpha_v\beta_3$ based on the X-ray crystal structure (Xiong et al., 2002). The two noncovalently associated subunits α_v (blue) and β_3 (magenta) bend into a compact form in the crystal structure, though the physiological relevance of this bend is highly debated (Arnaout et al., 2002; Takagi and Springer, 2002). A small cyclic RGDfNMeV peptide ligand (yellow) binds to this receptor at the interface between the β propeller of α_v and the βA domain (I-like domain) on β_3. Fragments missing in the crystal structure are represented by dashed lines. To orient the reader, a not-to-scale schematic cell membrane is shown.

(B and C) In our molecular dynamics study, only a complex comprised of the β propeller, βA, and hybrid domains were included, as indicated in (A) by the black dotted lines and shown in (B) the cartoon and (C) the surface representation. The complex, called integrin binding headpiece, was solvated in a periodic box containing (C) 44,300 water molecules (blue semitransparent lines) with 140,000 atoms overall.

in RGD integrin binding (Chen et al., 2003; Liddington, 2002; Mould et al., 2003).

To develop a high-resolution structural model that describes how binding of the RGD loop to integrins is stabilized, and why it can sustain considerable mechanical forces despite the shallowness of the binding site, we conducted molecular dynamics (MD) simulations. First, equilibrium MD simulations were used to investigate the contacts between the cyclic RGD peptide and the integrin binding site. Second, these were followed by nonequilibrium SMD simulations in which force was applied between a cyclic RGD peptide and the headpiece of the $\alpha_v\beta_3$ integrin to study the structural changes that occur as the RGD loop separates under force.

Results

The LIMBS Ion Coordinates to the MIDAS Bound Asp[RGD] during Equilibration

In our simulations, the crystal coordinates of the head of $\alpha_v\beta_3$ integrin, comprising the βA and the hybrid domains from the β_3 subunit, and the β propeller from the α_v subunit, bound to the cyclo-RGDfNMeV peptide, were equilibrated in a box filled with water molecules (Figure 1). The MD simulations were conducted over 1 ns (see

Figure 1) and yielded a stable system with the backbone heavy atom rmsd of <1.75 Å for both the β propeller and the βA domains.
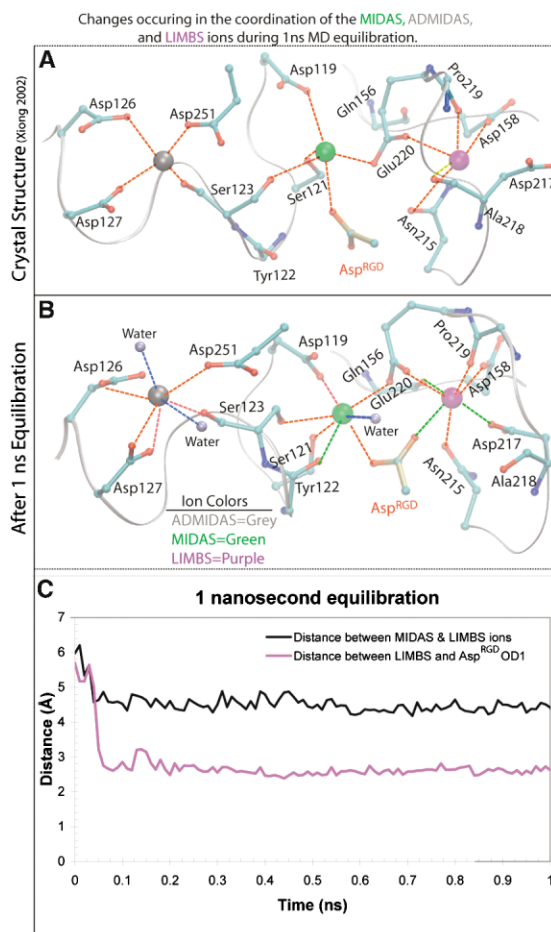
Several important structural changes were observed at the RGD binding site, while only minor changes were discernible in the integrin complex as a whole. The most significant change is that one of the two carboxylic oxygens from Asp[RGD] formed a new contact with the LIMBS ion within the first 10 ps of equilibration, while the other carboxylic oxygen of Asp[RGD] maintained its original contact with the MIDAS ion, as shown in Figures 2 and 3. Thus, during equilibration, Asp[RGD] contacted both the MIDAS and LIMBS ions (Figure 3C), whereas Asp[RGD] contacted only the MIDAS ion in the original crystal structure. As expected, water molecules that were not present in the original crystal structure coordinate to the solvent-accessible divalent cations, i.e., the MIDAS and ADMIDAS ions. Two water molecules are within 3 Å of the ADMIDAS ion, and one water molecule coordinates with the MIDAS ion (Figure 4).

Several observations indicate that coordination to the LIMBS ion is not an artifact of the chosen force fields. First, no major interactions between the integrin and RGD peptide or between the integrin and the MIDAS, LIMBS, and ADMIDAS ions were lost during equilibration
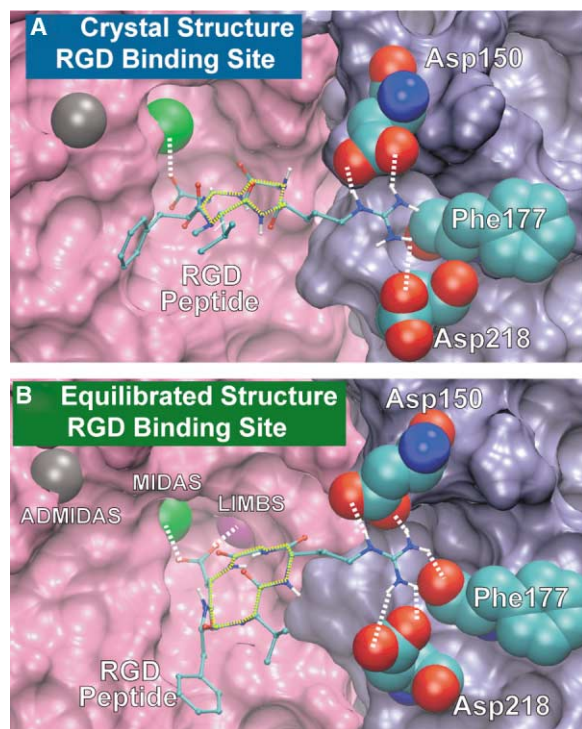
Figure 2. Snapshots of the RGD Binding Site of $\alpha_v\beta_3$

(A and B) Snapshots of (A) the original crystal structure and (B) after 1 ns of equilibration. During the equilibration, several new contacts are made with the cyclo-RGDfNMeV ligand. The aspartic acid (Asp[RGD]) amino acid makes a new contact with the LIMBS Mn^{2+} ion such that, after the equilibration, one carboxylate oxygen is coordinated by the MIDAS Mn^{2+} ion and the other carboxylate oxygen is coordinated by the LIMBS ion. In addition, both Asp218 and Phe177 make new contacts with the arginine of the cyclo-RGDfNMeV ligand (Arg[RGD]). Representations are chosen to show as much of the binding site as possible. Both the β_3 integrin subunit (magenta) and the α_v subunit (light blue) are shown in a surface representation. The cyclo-RGDfNMeV ligand is in a CPK representation. Amino acids from integrin $\alpha_v\beta_3$ that form salt bridges with the cyclo-RGDfNMeV ligand are shown in VDW representation (carbon atoms are cyan, nitrogen atoms are blue, oxygen atoms are red, and polar hydrogens are white; nonpolar hydrogen are not shown). The ADMIDAS (gray), MIDAS (green), and LIMBS (purple) ions are shown in VDW representations. Salt bridges and hydrogen bonds are shown as dotted white lines, and a backbone trace of the cyclo-RGDfNMeV peptide is shown as a yellow dotted line.

Figure 3. Coordination Spheres of the LIMBS, ADMIDAS, and MIDAS Mn^{2+} Ions

(A and B) Coordination spheres in the (A) crystal structure and (B) after 1 ns of equilibration. Atoms are shown with a CPK representation (carbon atoms are cyan, nitrogen ions are blue, and oxygen atoms are red; hydrogen atoms are not shown), and a portion of the integrin backbone connecting these amino acids is shown as a gray ribbon. The ADMIDAS (gray), MIDAS (green), and LIMBS (purple) ions are shown in VDW representation. Contacting atoms are shown as red dotted lines if no change occurred during equilibration, whereas yellow dotted lines indicate that a contact was broken during equilibration, blue lines indicate a contact with a water molecule, and green dotted lines indicate that a contact was made during equilibration.

(C) Distances between the MIDAS and LIMBS ions and between the LIMBS ion and the oxygen of the ASP[RGD] as a function of time during equilibration.

(see Figure 2). Given that the starting structure was solved at an rmsd of 3.2 Å, special care was taken to optimize side chain starting positions without affecting the backbone coordinates and also to insure that the electrostatics were modeled as rigorously as possible by using Particle Mesh Ewald (PME) full electrostatics rather than cutoffs. Indeed, it was found that Asp[218] and Phe[177] make new contacts with the arginine of the cyclo-RGDfNMeV ligand (Arg[RGD]), an interaction that is expected to be electrostatically favorable. In control simulations using cutoffs instead of a more rigorous PME electrostatics approach, coordination of the Asp to the LIMBS ion was seen, but other electrostatically favorable contacts to the Arg[RGD] were lost in this case from the original structure. These control simulations suggest that the use of full PME electrostatics provides more

accurate results and is essential for the present investigation. Taken together, our simulations show that interaction with the Asp of the cyclic RGD peptide and the LIMBS ion is structurally feasible. Second, the previously unpredicted coordination of Asp[RGD] from the cyclo-RGDfNMeV peptide with both of the MIDAS and LIMBS ions occurred repeatedly within the first few picoseconds of the equilibration without requiring substantial changes in the coordination spheres of the adhesion site ions. The only change in the MIDAS coordination sphere compared to the crystal structure is that one of the empty coordination positions is filled during equili-
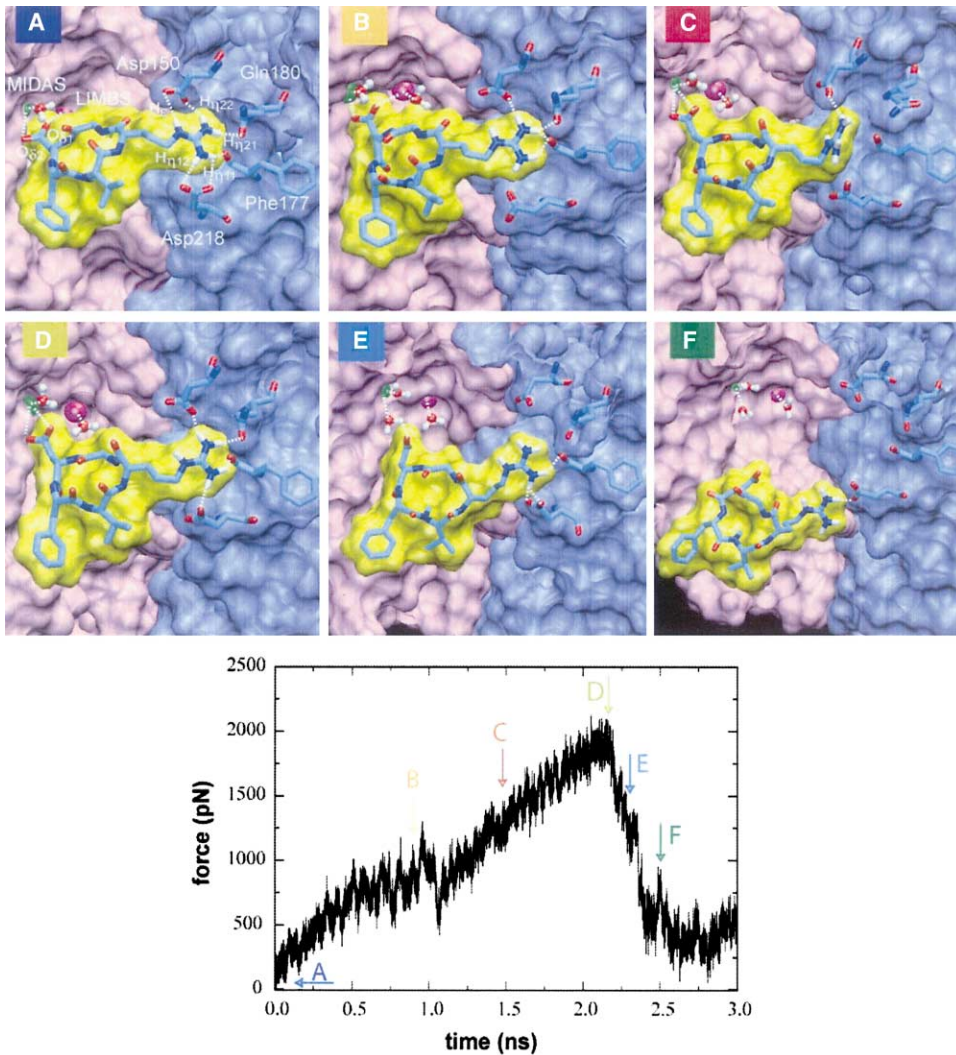
Figure 4. Sequential Snapshots of Pulling the Cyclo-RGDfNMeV Peptide out of the Binding Sites of $\alpha_v\beta_3$ at a Constant Velocity of 5 Å/ns

(A–F) The corresponding force-time curve is shown below (A)–(F). (A) A harmonic force was applied to the backbone C_α atoms of the ligand after the equilibration. (B and C) A water molecule (B) diffuses to a location near the LIMBS ion and (C) weakens the interaction between the LIMBS ion and one of carboxylic oxygens of Asp[RGD]. (D) Both carboxylic oxygen atoms of Asp[RGD] contact the MIDAS ion. Disrupting this contact results in the major force peak observed in the force-time curve. (E and F) The peak force corresponds to (E) the detachment of Asp[RGD] from the coordination sphere of the MIDAS ion, followed by smaller peaks corresponding to (F) the breaking of salt bridges between Arg[RGD] and the α_v subunit. Coloring is the same as in Figure 3, with the exception that all water molecules within 3 Å of the MIDAS ion, LIMBS ion, and Asp[RGD] carboxylic oxygens (Asp[RGD]:OD1, Asp[RGD]:OD2) are shown as red (oxygen) and white (hydrogens) spheres. Also, the cyclo-RGDfNMeV peptide is shown as a yellow surface representation overlayed by a ball and stick representation to show the positions of its atoms.

bration by a water molecule (Figure 3B), as would be energetically expected. Furthermore, the coordination sphere of the LIMBS ion experiences only minor changes. While Asp[217] (of α_v) was initially coordinated to the LIMBS ion via its backbone oxygen in the crystal structure, it coordinates the LIMBS ion via its two (only one is visible in Figure 3C due to the snapshot orientation) side chain carboxylic oxygens after equilibration. The backbone oxygen of Glu[156] filled an empty coordination position at approximately 100 ps and through the rest of the 1 ns equilibration. Upon cocoordinating Asp[RGD], the distance between the MIDAS and LIMBS ions decreased from 5.9 to 4.5 Å, and Glu[220] moved

slightly, such as to not reside directly between the LIMBS and MIDAS ions. Altogether, the cocoordination of Asp[RGD] required only very minor changes at the binding sites of the LIMBS and MIDAS ions.

Role of Different Divalent Cations
To investigate the role of different divalent cations and of different numbers of water molecules coordinated to the MIDAS ion, we first simulated the integrin complex as described by replacing the Mn^{2+} ions with Ca^{2+} ions. Because of the relatively short (nanosecond) simulation time, the Ca^{2+} ions would not dissociate. In the presence of Ca^{2+} rather than Mn^{2+}, Asp[RGD] coordinated only with

the MIDAS ion in two simulations, consistent with the crystal structure, whereas the two carboxylic oxygens of Asp^{RGD} coordinated with both the LIMBS and MIDAS ions in only one of the three simulations. Second, we confirmed that MIDAS Mn^{2+} ion coordination to one water molecule is critical to the events described here.

Recent crystal structures of the open form of the αM and α2 I/A domains suggest that the MIDAS ion is coordinated by two water molecules (Emsley et al., 2000; Lee et al., 1995B). However, in the original crystal structure of α$_v$β$_3$, such water molecules were not resolved. To address this issue, an additional simulation was conducted in which we placed two water molecules coordinating the MIDAS Mn^{2+} ion by aligning the β3 I/A domain to the αM I/A domain (see the Experimental Procedures). After a 1 ns equilibration, only one of the two water molecules remained bound to the MIDAS ion; the structure encompassing the RGD binding site remained unaltered through the equilibration.

New Contact Formed between Arg^{RGD} with the α$_v$ Subunit during Equilibration

While all three metal binding sites are located on the β$_3$ subunit, new stabilizing contacts were formed between the Arg^{RGD} and the α$_v$ subunit (see Figure 2). Arg^{RGD} maintains its bidentate salt bridge between Arg^{RGD}:H$_ε$ and Arg^{RGD}:H$_{η22}$ and the carboxylic oxygens of Asp^{150} on α$_v$. However, a new bidentate salt bridge forms between Arg^{RGD}:H$_{η11}$ and Arg^{RGD}:H$_{η12}$ and Asp^{150} on α$_v$, whereas only one salt bridge from Arg^{RGD}:H$_{η11}$ was observed between these amino acids in the crystal structure. A new hydrogen bond is also formed between Arg^{RGD} and the side chain oxygen of Gln^{180} and the backbone oxygen of Phe^{177} (contact to Gln^{180} is shown in Figure 4A). Thus, Arg^{RGD} maintains its original interactions and gains new stabilizing ionic interactions with neighboring polar or charged amino acids located on the α$_v$ subunit.

Overall, the original contacts between the cyclo-RGDfNMeV ligand and α$_v$β$_3$ were well maintained throughout the course of the equilibration. However, new contacts emerged during the equilibration with both the α$_v$ and β$_3$ subunits, suggesting that the cyclo-RGDfNMeV ligand is in a more stable conformation after equilibrating the crystal structure in a box filled with water molecules.

Forced Unbinding of RGD from α$_v$β$_3$ Integrin

To induce the unbinding of the cyclo-RGDfNMeV ligand from the integrin binding site, we adopted a well-established computational procedure (Isralewitz et al., 2001) and applied a harmonic constraint to the ligand, thereby pulling it from the integrin binding site at constant velocity (cv-SMD). This type of simulation has previously been shown to elucidate key structural features of force-induced receptor-ligand unbinding pathways (Grubmuller et al., 1996; Izrailev et al., 1997). Figure 4 presents the key steps of the unbinding events identified in a cv-SMD simulation of the cyclo-RGDfNMeV ligand from α$_v$β$_3$ at a velocity of 5 Å/ns.

Upon pulling on the cyclo-RGDfNMeV ligand, the first major structural event is the breaking of the contact between Asp^{RGD} and the LIMBS ion, the interaction that

had formed during equilibration. This coincides with a slight reorientation of Asp^{RGD} so that both of its carboxylic oxygens contact only the MIDAS ion (Figure 4C). This event typically revealed itself in SMD as a shoulder in the major force peak in the force versus displacement curve. Here, displacement refers to the distance between the center of mass of the five C$_α$ atoms of the cyclo-RGDfNMeV peptide from its equilibrated coordinate position. In all simulations conducted at various pulling speeds, the major force peak consistently correlated with the breaking of the contact between Asp^{RGD} and the MIDAS ion (Figure 4D and see below). It is important to realize (and discussed in more detail below) that breaking of the cyclo-RGDfNMeV contact with the integrin is accomplished through attacks from surrounding water molecules, which appear to compete for the carboxylic oxygen of Asp^{RGD} that normally interacts only with the MIDAS ion.

During the pull, the four salt bridges and one hydrogen bond between Arg^{RGD} and the α$_v$ subunit were broken individually, one by one, both concomitant to the major force peak and subsequent. As seen in Figure 4, one of the two salt bridge contacts between Asp^{150} and Arg^{RGD}, and two contacts between Asp^{218} and Arg^{RGD} were first disrupted (Figure 4B). The detachment of Arg^{RGD} from Asp^{150}, Gln^{180}, and Phe^{177} coincides with the major peak, whereas in other simulations, this detachment occurred later in the trajectory, resulting in smaller peaks following the major peak. Similar to their role in breaking of the Asp^{RGD}-MIDAS contacts, water molecules were found to compete with and attack the salt bridges connecting Arg^{RGD} to the integrin, facilitating its detachment. Overall, inspection of the force-displacement curves shows that breaking of these salt bridges does not lead to substantial force peaks. Likewise, the corresponding structural data show that these salt bridges are under frequent attack by water molecules due to their high solvent accessibility.

Coordination of Water to the Divalent MIDAS Ion Stabilizes the Asp^{RGD}-α$_v$β$_3$ Interaction

Water molecules participate actively in the unbinding process of the cyclo-RGDfNMeV ligand from α$_v$β$_3$. The salt bridges formed between the Arg^{RGD} side chain and the α$_v$ subunit are among the first to break. An analysis of the number of collision events between water molecules and the five hydrogen atoms on the tip of the Arg^{RGD} side chain shows that all these hydrogen atoms are quite accessible to water. The frequent attacks of these hydrogen atoms by water molecules result in a destabilization of the salt bridges formed between the Arg^{RGD} side chain and the α$_v$ subunit (Figures 5A–5E).

The breaking of the Arg^{RGD} salt bridges requires significantly less force than needed for the disruption of the contacts between the MIDAS ion and Asp^{RGD}. While the hydrogens on Arg^{RGD} were contacted up to five times per picosecond by water molecules, very few water collisions occur between free water molecules and the carboxylic oxygen of Asp^{RGD} that coordinates to the MIDAS ion, or between free water molecules and the MIDAS ion itself (Figures 5E and 5G). The attacks on the carboxylic oxygen of Asp^{RGD} increase in frequency as the carboxylic
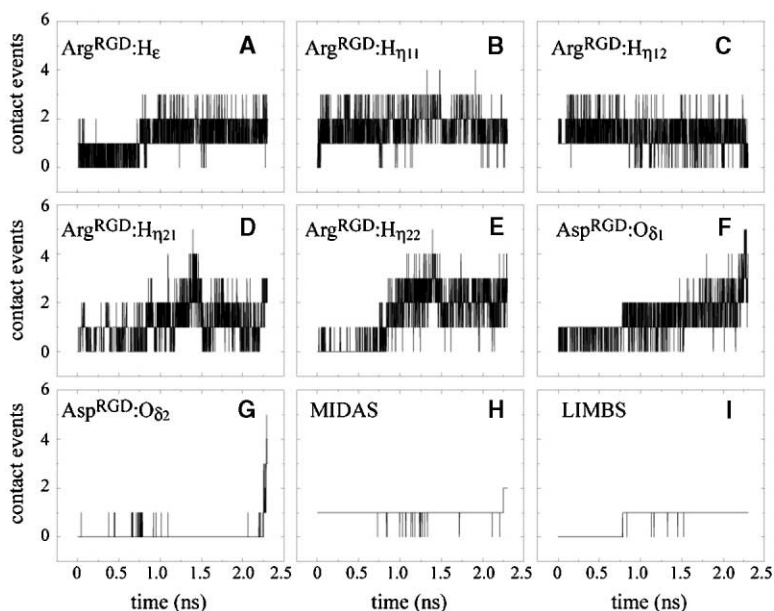
Figure 5. Number of Water Contacts to Key Atoms of the Binding Pocket during the SMD Unbinding Simulation of the RGD-$\alpha_v\beta_3$ Integrin Complex

(A–I) Positions of these key atoms are shown in Figure 4A. For each time step (at picosecond intervals), the contacts to a specified atom were counted by identifying the number of water molecules within 3 Å of the specified atom. (A–E) Contacts to five hydrogen atoms on the Arg side chain of the RGD ligand (Arg^{RGD}). (F and G) Number of contacts of water molecules with (F) the carboxylic oxygen atom on the Asp^{RGD}, which is coordinated to the LIMBS Mn^{2+} ion, and with (G) the Asp^{RGD} carboxylic oxygen atom, which is coordinated to the MIDAS Mn^{2+} ion. (H and I) Water contacts to the Mn2+ ions at the MIDAS and LIMBS ions, respectively. Data are from the same simulation as presented in Figure 4.

oxygen of Asp^{RGD} is separating from the MIDAS ion. In contrast, the exposure to water attacks of the second carboxylic oxygen of Asp^{RGD} that initially coordinated to the LIMBS ion upon equilibration is significantly higher (Figure 5F), which explains their early dissociation under force.

Why is the bond formed between the Asp^{RGD} and the MIDAS ion relatively well protected from water attacks? This major force-bearing bond has to be broken before the RGD peptide can separate from the integrin. The equilibrated structure shows that a water molecule coordinated by the MIDAS ion is just 3–4 Å away from Asp^{RGD}. During pulling, this water molecule comes occasionally within 3 Å of the oxygen of Asp^{RGD} but does not break the Asp^{RGD}-MIDAS ion contact (Figure 5G). Instead of competing for the oxygen of Asp^{RGD}, this water molecule remains preferentially coordinated to the MIDAS ion. It is not until both an additional water molecule comes within 3 Å of the Asp^{RGD}'s oxygen and the cyclo-RGDfNMeV has stretched 5–6 Å out of it's binding pocket that the Asp^{RGD}-MIDAS contact breaks coincidently with the major force peak. Thus, the tightly coordinated water molecule blocks the path through which other water molecules would access and attack the most critical force-bearing bond, thereby shielding the Asp^{RGD}-Mn^{2+} contact from competition with free water molecules. The ability of Mn^{2+} to coordinate water could thus be one structural reason why RGD sequences can remain bound to the shallow crevice formed between the $\alpha_v\beta_3$ subunits even under mechanical force.

Testing the Structural Hypothesis of How the RGD-$\alpha_v\beta_3$ Interactions Are Stabilized Mechanically

In studying the structural basis of the receptor-ligand interactions, the force fields of selected atoms may be turned off to test their significance. To investigate the hypothesis that the RGD-$\alpha_v\beta_3$ interactions are mechanically stabilized by coordination of a water molecule to

the divalent MIDAS ion, additional SMD simulations were conducted to probe unbinding, during which we turned off the electrostatic interaction of the MIDAS ion (denoted as ΔMIDAS), the LIMBS ion (ΔLIMBS), both the MIDAS and LIMBS ions (ΔMIDAS-ΔLIMBS), the five hydrogens of the Arg^{RGD} contacting the α_v subunit (ΔArg^{Elec}), and all the above components (ΔMIDAS-ΔLIMBS-ΔArg^{Elec}), as shown in Figure 6. In the ΔLIMBS simulation, the primary force peak was reduced by only 8% since Asp^{RGD} reoriented such that its carboxylic oxygen contacted only the MIDAS ion. In contrast, when we turned off the charge of the divalent MIDAS ion (ΔMIDAS), the Asp^{RGD} reoriented to coordinate to the LIMBS ion, and the major force peak was reduced by 31%. Elimination of the charges on both divalent ions (ΔMIDAS-ΔLIMBS) reduced the force peak by 27%. When we turned off the charges on the Asp^{RGD} oxygens (ΔArg^{Elec}), the force peak was reduced by 20%. Finally, turning off all the above specified charges simultaneously (ΔMIDAS-ΔLIMBS-ΔArg^{Elec}) caused the largest reduction of the maximal force, namely, by 50%. Taken together, these simulations demonstrate that the electrostatic interaction between the divalent cations and the carboxylate oxygen of Asp^{RGD} are essential for the stabilization of the noncovalent bond between RGD and integrin $\alpha_v\beta_3$. As previously discussed, the absolute height of the force peak depends on the pulling velocity and barrier shape and will be lower at physiological loading rates (Craig et al., 2004; Evans, 2001). While these simulations cannot predict absolute forces required for detachment at physiological conditions, they can provide critical insight into the interactions furnishing mechanical stability.

Discussion

A principle challenge in integrin biology is to reveal the structural basis for integrin binding and activation. Molecular dynamics simulations provide for the first time,
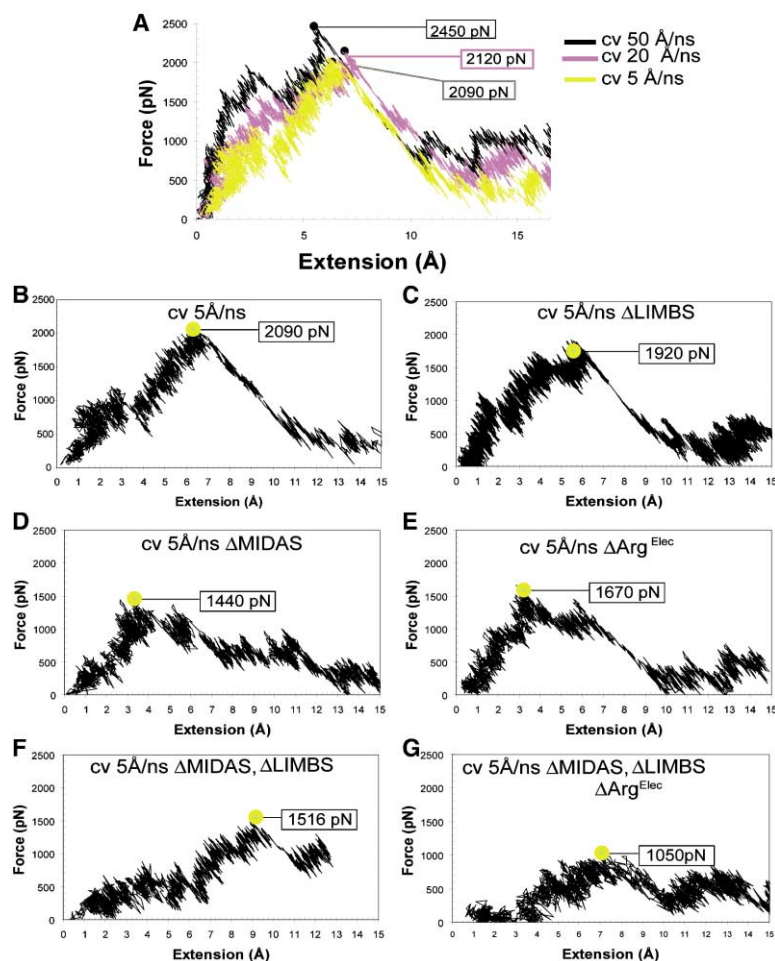
Figure 6. Comparison of the Mechanical Stabilities of the Wild-Type RGD-$\alpha_v\beta_3$ Integrin Complex to Various Artificial Complexes

(A) Force-displacement curves at pulling velocities of 5–50 Å/ns for the wild-type. Displacement is defined as the distance separating the center of mass of the C$_\alpha$ atoms of the cyclo-RGDfNMeV peptide from their original position. Typically, one major force peak was observed, followed by smaller subpeaks. The major force peak corresponds to the breaking of the contact between the MIDAS ion and the carboxylate atom(s) of Asp^{RGD}. A shoulder on the main force peak was typically observed and corresponded to the breaking of the contact between one (but not both) of the carboxylate oxygens of Asp^{RGD} with a divalent cation. Variations were observed in the smaller force peaks, which generally corresponded to the breaking of individual salt bridges between amino acids of α_v and Arg^{RGD}.

(B–G) Force-displacement curves at 5 Å/ns for the wild-type and various artificial complexes. The electrostatic component of the MIDAS, LIMBS, and/or five hydrogen atoms on the tip of the Arg^{RGD} side chain is turned off. The respective simulations are denoted as ΔMIDAS, ΔLIMBS, ΔArg^{Elec}, or a combination of these three.

to our knowledge, structural insight into several critical functions of the divalent cations in stabilizing the RGD-$\alpha_v\beta_3$ complex, functions that are not apparent from the static crystal structure alone.

One consistent finding in our simulations was that the Asp^{RGD} of the cyclic RGD peptide is coordinated not only to the MIDAS ion but also to the LIMBS ion, an interaction that was not anticipated from the crystal structure and forms early in the equilibration. Upon pulling on the cyclo-RGDfNMeV ligand, the contact between Asp^{RGD} and the LIMBS ion is among the first to break. In recent experimental studies in which no force was applied to the RGD integrin complex, Springer and colleagues concluded that the LIMBS site positively regulates ligand binding to the MIDAS site (Chen et al., 2003). While not apparent from the crystal structure, we see in our molecular dynamics simulations that one of the carboxylic oxygens of Asp^{RGD} directly coordinates to the LIMBS ion, thereby providing a structural explanation for how the LIMBS ion might act as a positive regulator of ligand binding. It is also interesting to note that $\alpha_v\beta_3$ and $\alpha_5\beta_1$ are key integrins mediating force-regulated cell adhesion and anchoring to the extracellular matrix (Katz et al., 2000; Zamir and Geiger, 2001). While they lack the I domain in the α integrin, they bind RGD ligands via the MIDAS site located on the I-like domain of the β subunit. Ligand binding of other integrins such as $\alpha_L\beta_2$

is mediated by the MIDAS ion of the I domain. While no LIMBS ion is found next to the ligand binding MIDAS site of the I domain, it is the second MIDAS site on the I-like domain of those other integrins that regulates ligand binding by the I domain (Yang et al., 2004). Future studies will have to reveal how the ability of Asp^{RGD} to coordinate to the LIMBS ion relates to the structure of the protein scaffold in which the RGD is presented.

Forced separation of RGD-containing peptides or proteins from either $\alpha_v\beta_3$ or $\alpha_5\beta_1$ integrins ($\alpha_5\beta_1$-fibronectin and $\alpha_v\beta_3$-echistatin) required tens to hundreds of pN (Lehenkari and Horton, 1999; Li et al., 2003). The bend in integrin $\alpha_v\beta_3$'s quaternary structure, observed in crystal structures (see Figure 1) where the head piece is bent down toward the membrane, has led to many suggestions of how changes in the overall quaternary and tertiary structure could potentially "activate" integrin binding to RGD proteins (Gottschalk and Kessler, 2002; Liddington, 2002; Luo et al., 2004; Takagi et al., 2002; Xiong et al., 2003). It is still debated whether the bending in integrin $\alpha_v\beta_3$ is an artifact of crystallization and whether it is connected with an inactivated or activated form. Ideally, one would like to compare the rupture force calculated in SMD simulations to that probed in experiments. However, due to the differences in time scale at which the events are probed, forces derived from SMD simulations can only be compared with exper-

imental data if sufficient experimental information is available regarding the potential barrier width (Craig et al., 2004). Otherwise, potential of mean force calculations (Gullingsrud et al., 1999; Park and Schulten, 2004) are needed which would go far beyond the scope of this paper.

The present study provides the explanations derived from SMD regarding the mechanism of how divalent cations stabilize the interactions formed between integrin $\alpha_v\beta_3$ and the RGD peptide across a shallow crevice. While the key force-bearing hydrogen bonds are not buried in a deep binding pocket that would protect them from water attacks, the simulations show that one water molecule, tightly coordinated to the divalent MIDAS ion, is effectively blocking further access of water to critical force-bearing interactions. For other systems, it has already been shown that the mechanical stability of force-bearing hydrogen bonds is enhanced if shielded from water molecules that would otherwise compete for the hydrogen bonding partners forming the linkages (Craig et al., 2004; Lu and Schulten, 2000). Considering the critical role integrins play in mechanotransduction, the mechanical stability of the entire adhesion complex that includes all integrin linkages to the ECM and the cytoskeleton is only as strong as its weakest link. Our simulations give structural insights into how the RGD integrin linkage is mechanically stabilized by the MIDAS ion. Since peptide sequences flanking the RGD impact integrin selectivity and binding strength, as recently reviewed in (Hersel et al., 2003), additional shielding of force-bearing bonds might occur for other RGD peptides and especially for RGD proteins that have an increased total contact area with their integrins (Krammer et al., 2002; Redick et al., 2000). Shielding of force-bearing residues and formation of new contacts between ligand and integrin will certainly affect the energy barrier height. However, the final event in separating the RGD loop from integrin in all of these cases will be defined by the rupture of the Asp^{RGD} from the MIDAS ion that we have structurally described here.

While observed here for integrin $\alpha_v\beta_3$, the functional role of a water molecule tightly coordinated to the MIDAS ion might reflect a general principle of how divalent cations stabilize receptor-ligand interactions. The MIDAS motif is found on all of the 8 human β integrins and on 9 of the 18 known human α integrins ($\alpha1$, $\alpha2$, $\alpha10$, $\alpha11$, αD, αX, αM, αL, and αE) (Whittaker and Hynes, 2002). As for integrins, the MIDAS motif is common to many other proteins that contain the phylogenetically ancient von Willebrand A (vWA) domain. This includes the anthrax toxin receptor (Bradley et al., 2003; Santelli et al., 2004), various calcium and chloride channels, complement factors, protease inhibitors, the family of vWA collagens, and the cytoplasmic vault ribonucleoprotein complex (Whittaker and Hynes, 2002). Altogether, the vWA domain has been identified in 500 extra- and intracellular proteins, many of which have MIDAS motifs (Whittaker and Hynes, 2002).

Is tight coordination of water molecules to divalent ions a ubiquitous mechanism by which those receptor-ligand interactions that form shallow crevices rather than deep pockets are shielded from attacks by free water molecules? One can speculate whether the physi-

ological advantage of shallow crevices compared to a deep binding site might be that a shallow binding site topography facilitates access to the binding partner, thus enhancing the on-rate. However, a shallower interface between the partners will also increase access of free water molecules, which would undermine the stability of the complex unless the complex is stabilized by other means. While shallow binding sites might allow for faster on-rates, potentially even further accelerated by the presence of the charge, divalent ions could play an additional critical role of shielding crucial interactions from attack by free water molecules, thus enhancing the barrier of dissociation. While the regulatory functions of divalent cations have been well recognized, the structural reasons behind the stabilization of receptor-ligand interactions by divalent cations are still largely unknown.

Experimental Procedures

The extracellular portion of integrin $\alpha_v\beta_3$, together with a cyclo-RGDfNMeV ligand bound to the integrin, was adopted from the crystallographic structure determined at 3.2 Å resolution (Protein Data Bank entry code 1L5G [Xiong et al., 2002]). To reduce the size of the system, domains other than the βA, hybrid, and the β propeller domains were removed, since we are primarily studying interaction between the RGD peptide and its binding pocket. The remaining parts were subsequently solvated in a TIP3 (Jorgensen, 1983) water cell of size $130 \times 130 \times 120$ Å^3. Water molecules within 2.5 Å of the protein were removed, resulting in a system of 146,291 atoms. The Mn^{2+} cations in the original crystal structure were included in the solvated structure. Seven additional divalent ions were introduced to neutralize the system. MD simulations were then carried out with the program NAMD (Kale et al., 1999). An Accelerys version of the CHARMM22 force fields was utilized (MacKerell, 1998). This particular version of the CHARMM force field, as compared to the academic version, was used because it included a parameter set describing the Mn^{2+} cation. While all the starting coordinates for the oxygen, carbon, and for the cyclo-RGDfNMeV bound to integrin $\alpha_v\beta_3$ were taken from the crystal structure, the patch "LINK" was used with the program PSFGEN in the NAMD2 package to create the peptide bond between the Phe and Val. The patch "NPME" was used to generate the N-methylation site on Val. Parameters for the L-form Phe were employed for the D-amino acid Phe (fN) of the cyclic peptide since these two isomers are chemically identical and no special parameters for the D-form are available. A similar approach was taken in MD simulations of the cyclo-ligand alone (Dechantsreiter et al., 1999).

The system was first minimized for 2 consecutive 2,000 conjugate gradient steps, where the protein was held fixed and water molecules were allowed to move; then, all atoms were allowed to move. After minimization, the system was gradually heated from 0 K to 300 K in 30 ps and subsequently equilibrated for 1 ns under constant pressure and temperature conditions (NPT). The pressure was maintained at 1 atm by using the Langevin piston method (Feller et al., 1995), and the temperature was controlled by using Langevin dynamics at 300 K with a damping coefficient of 5 ps^{-1}. A piston period of 100 fs and a damping time constant of 50 fs were employed for the pressure control. To prevent drifting, the backbone C_α atoms of both C termini residues Arg^{438} on the α subunit and Asp^{432} on the β subunit were fixed. During 1 ns of equilibration, the system exhibited an all-atom rmsd of less than 2.5 Å for both subunits. No water molecules were resolved in the original crystal structure. During 1 ns of equilibration, only one water molecule was found coordinated to the MIDAS ion. A second water molecule has been found to coordinate the MIDAS Mn^{2+} ion in other crystallographic studies of integrin structures (Emsley et al., 2000; Lee, 1995A). By aligning residues (Asp^{119}, Ser^{121}, and Ser^{123}) coordinating the MIDAS site of α_v to those (Asp^{140}, Ser^{142}, and Ser^{144}) of α_M (PDB code 1IDO), we placed two water molecules in the proximity of the MIDAS ion in order to carry out a control simulation.

External forces were applied to pull the RGD ligand away from the integrin binding site by means of constant velocity SMD simulations (cv-SMD). Pulling velocities of 5 Å/ns and 20 Å/ns were used. The center of mass R_c of the ligand cyclo-RGDfNMeV was harmonically constrained with a force of $F = k(vt - x)$, where k is the spring constant, v is the velocity, and t is the time. The spring constant was set to 10 k_BT/Å^2. The direction of the force was chosen by the sum of two vectors, pointing from the two fixed C$_\alpha$ atoms on the α/β subunits to R_c. The variable x is the coordinate along the chosen direction of the force. The corresponding methods are reviewed in (Isralewitz et al., 2001).

Transient electrostatic interactions may be formed during detachment of the cyclo-RGDfNMeV peptide, resulting in smaller force peaks that were unique to a particular simulation. In these cases, a second simulation was conducted with a different pulling vector to verify that the smaller peaks were not omnipresent. For the computational mutant, ΔMIDAS-ΔLIMBS-ΔARG^{Elec}, a second simulation was conducted to resolve whether or not a small peak of 1,250 pN from a transient interaction with Arg^{RGD} was reproducible. As expected, the transient interaction was not observed, and the small peak was reduced to 1,050 pN in the second simulation.

Periodic boundary conditions were imposed for all MD simulations. Full electrostatics were computed every 4 fs by using the Particle Mesh Ewald (PME) method (Darden et al., 1993) with a grid spacing of less than 1.0 Å. In two control equilibrations using cutoff for electrostatics, the electrostatics were smoothly switching off between 10 Å and 12 Å and between 8 Å and 12 Å, respectively. Van der Waals interactions were gradually turned off at a distance between 10 Å and 12 Å. An integration time step of 1 fs and a uniform dielectric constant of 1 were chosen. Simulations lasting altogether 23 ns were completed at the Pittsburgh Supercomputing Center (PSC), on the Translational Genomics Research Institute, Arizona State University IBM 1024 node 2.5 GhZ Xeon processor computers, and on local Linux clusters. 1 ns simulation required 40 hr on 32 Compaq Alphaserver ES45 nodes (128 1GHz processors). During simulations, atomic coordinates of the whole system were saved for every picosecond of the simulation. Visualization and analysis of the trajectories were conducted by using VMD (Humphrey et al., 1996).

Supplemental Data

Supplemental Data including a movie representing a molecular dynamics simulation of pulling the cyclic cyclo-RGDfNMeV ligand from the binding pocket of integrin $\alpha_v\beta_3$ are available at http://www.structure.org/cgi/content/full/12/11/2049/DC1/.

References

Arnaout, M.A., Goodman, S.L., and Xiong, J.P. (2002). Coming to grips with integrin binding to ligands. Curr. Opin. Cell Biol. *14*, 641–651.

Baneyx, G., Baugh, L., and Vogel, V. (2002). Supramolecular chemistry and self-assembly special feature: fibronectin extension and unfolding within cell matrix fibrils controlled by cytoskeletal tension. Proc. Natl. Acad. Sci. USA *99*, 5139–5143.

Bradley, K.A., Mogridge, J., Jonah, G., Rainey, A., Batty, S., and Young, J.A. (2003). Binding of anthrax toxin to its receptor is similar to alpha integrin-ligand interactions. J. Biol. Chem. *278*, 49342–49347.

Chen, J., Salas, A., and Springer, T.A. (2003). Bistable regulation of integrin adhesiveness by a bipolar metal ion cluster. Nat. Struct. Biol. *10*, 995–1001.

Craig, D., Gao, M., Schulten, K., and Vogel, V. (2004). Tuning the mechanical stability of fibronectin type III modules through sequence variations. Structure (Camb.) *12*, 21–30.

Darden, T., York, D., and Pedersen, L. (1993). Particle Mesh Ewald—an N.Log(N) method for ewald sums in large systems. J. Chem. Phys. *98*, 10089–10092.

Dechantsreiter, M.A., Planker, E., Matha, B., Lohof, E., Holzemann, G., Jonczyk, A., Goodman, S.L., and Kessler, H. (1999). N-methylated cyclic RGD peptides as highly active and selective alpha(v)beta(3) integrin antagonists. J. Med. Chem. *42*, 3033–3040.

Emsley, J., Knight, C.G., Farndale, R.W., Barnes, M.J., and Liddington, R.C. (2000). Structural basis of collagen recognition by integrin alpha2beta1. Cell *101*, 47–56.

Evans, E. (2001). Probing the relation between force–lifetime–and chemistry in single molecular bonds. Annu. Rev. Biophys. Biomol. Struct. *30*, 105–128.

Feller, S.E., Zhang, Y.H., Pastor, R.W., and Brooks, B.R. (1995). Constant-pressure molecular-dynamics simulation—the Langevin Piston method. J. Chem. Phys. *103*, 4613–4621.

Galbraith, C.G., Yamada, K.M., and Sheetz, M.P. (2002). The relationship between force and focal complex development. J. Cell Biol. *159*, 695–705.

Giannone, G., Jiang, G., Sutton, D.H., Critchley, D.R., and Sheetz, M.P. (2003). Talin1 is critical for force-dependent reinforcement of initial integrin-cytoskeleton bonds but not tyrosine kinase activation. J. Cell Biol. *163*, 409–419.

Gottschalk, K.E., and Kessler, H. (2002). The structures of integrins and integrin-ligand complexes: implications for drug design and signal transduction. Angew. Chem. Int. Ed. Engl. *41*, 3767–3774.

Grubmuller, H., Heymann, B., and Tavan, P. (1996). Ligand binding: molecular mechanics calculation of the streptavidin-biotin rupture force. Science *271*, 997–999.

Gullingsrud, J.R., Braun, R., and Schulten, K. (1999). Reconstructing potentials of mean force through time series analysis of steered molecular dynamics simulations. J. Comput. Phys. *151*, 190–211.

Hersel, U., Dahmen, C., and Kessler, H. (2003). RGD modified polymers: biomaterials for stimulated cell adhesion and beyond. Biomaterials *24*, 4385–4415.

Humphrey, W., Dalke, A., and Schulten, K. (1996). VMD—visual molecular dynamics. J. Mol. Graph. *14*, 33–38.

Hyre, D.E., Amon, L.M., Penzotti, J.E., Le Trong, I., Stenkamp, R.E., Lybrand, T.P., and Stayton, P.S. (2002). Early mechanistic events in biotin dissociation from streptavidin. Nat. Struct. Biol. *9*, 582–585.

Isralewitz, B., Gao, M., and Schulten, K. (2001). Steered molecular dynamics and mechanical functions of proteins. Curr. Opin. Struct. Biol. *11*, 224–230.

Izrailev, S., Stepaniants, S., Balsera, M., Oono, Y., and Schulten, K. (1997). Molecular dynamics study of unbinding of the avidin-biotin complex. Biophys. J. *72*, 1568–1581.

Jorgensen, W.L., Chandrasekhar, J., Madura, J.D., Impey, R.W., and Klein, M.L. (1983). Comparison of simple potential functions for simulating water. J. Chem. Phys. *79*, 926–935.

Kalé, L., Skeel, R., Bhandarkar, M., Brunner, R., Gursoy, A., Krawetz, N., Phillips, J., Shinozaki, A., Varadarajan, K., and Schulten, K. (1999). NAMD2: greater scalability for parallel molecular dynamics. J. Comp. Phys. *151*, 283–312.

Katz, B.Z., Zamir, E., Bershadsky, A., Kam, Z., Yamada, K.M., and Geiger, B. (2000). Physical state of the extracellular matrix regulates the structure and molecular composition of cell-matrix adhesions. Mol. Biol. Cell *11*, 1047–1060.

Krammer, A., Craig, D., Thomas, W.E., Schulten, K., and Vogel, V. (2002). A structural model for force regulated integrin binding to fibronectin's RGD-synergy site. Matrix Biol. *21*, 139–147.

Lee, J.O., Bankston, L.A., Arnaout, M.A., and Liddington, R.C. (1995A). Two conformations of the integrin A-domain (I-domain): a pathway for activation? Structure (Camb.) 3, 1333–1340

Lee, J.O., Rieu, P., Arnaout, M.A., and Liddington, R. (1995B). Crystal structure of the A domain from the alpha subunit of integrin CR3 (CD11b/CD18). Cell 80, 631–638.

Lehenkari, P.P., and Horton, M.A. (1999). Single integrin molecule adhesion forces in intact cells measured by atomic force microscopy. Biochem. Biophys. Res. Commun. 259, 645–650.

Li, F.Y., Redick, S.D., Erickson, H.P., and Moy, V.T. (2003). Force measurements of the alpha(5)beta(1) integrin-fibronectin interaction. Biophys. J. 84, 1252–1262.

Liddington, R.C. (2002). Will the real integrin please stand up? Structure (Camb.) 10, 605–607.

Lu, H., and Schulten, K. (2000). The key event in force-induced unfolding of Titin's immunoglobulin domains. Biophys. J. 79, 51–65.

Luo, B.H., Takagi, J., and Springer, T.A. (2004). Locking the beta3 integrin I-like domain into high and low affinity conformations with disulfides. J. Biol. Chem. 279, 10215–10221.

MacKerell, A.D., Bashford, D., Bellot, M., Dunbrack, R.L., Jr., Evansec, J., Field, M.J., Fischer, S., Gao, J., Guo, H., Ha, S., et al. (1998). All-hydrogen empircal potential for molecular modeling and dynamics studies of proteins using the CHARMM22 force field. J. Phys. Chem. B 102, 3586–3616.

Mould, A.P., Barton, S.J., Askari, J.A., Craig, S.E., and Humphries, M.J. (2003). Role of ADMIDAS cation-binding site in ligand recognition by integrin {alpha}5{beta}1. J. Biol. Chem. 278, 51622–51629.

Park, S., and Schulten, K. (2004). Calculating potentials of mean force from steered molecular dynamics simulations. J. Chem. Phys. 120, 5946–5961.

Redick, S.D., Settles, D.L., Briscoe, G., and Erickson, H.P. (2000). Defining fibronectin's cell adhesion synergy site by site-directed mutagenesis. J. Cell Biol. 149, 521–527.

Santelli, E., Bankston, L.A., Leppla, S.H., and Liddington, R.C. (2004). Crystal structure of a complex between anthrax toxin and its host cell receptor. Nature 430, 905–908.

Shimaoka, M., Takagi, J., and Springer, T.A. (2002). Conformational regulation of integrin structure and function. Annu. Rev. Biophys. Biomol. Struct. 31, 485–516.

Takagi, J., and Springer, T.A. (2002). Integrin activation and structural rearrangement. Immunol. Rev. 186, 141–163.

Takagi, J., Petre, B.M., Walz, T., and Springer, T.A. (2002). Global conformational rearrangements in integrin extracellular domains in outside-in and inside-out signaling. Cell 110, 599–611.

Thoumine, O., Kocian, P., Kottelat, A., and Meister, J.J. (2000). Short-term binding of fibroblasts to fibronectin: optical tweezers experiments and probabilistic analysis. Eur. Biophys. J. 29, 398–408.

Whittaker, C.A., and Hynes, R.O. (2002). Distribution and evolution of von Willebrand/integrin A domains: widely dispersed domains with roles in cell adhesion and elsewhere. Mol. Biol. Cell 13, 3369–3387.

Xiong, J.P., Stehle, T., Diefenbach, B., Zhang, R., Dunker, R., Scott, D.L., Joachimiak, A., Goodman, S.L., and Arnaout, M.A. (2001). Crystal structure of the extracellular segment of integrin alpha Vbeta3. Science 294, 339–345.

Xiong, J.P., Stehle, T., Zhang, R., Joachimiak, A., Frech, M., Goodman, S.L., and Arnaout, M.A. (2002). Crystal structure of the extracellular segment of integrin {alpha}V{beta}3 in complex with an Arg-Gly-Asp ligand. Science 296, 151–155.

Xiong, J.P., Stehle, T., Goodman, S.L., and Arnaout, M.A. (2003). New insights into the structural basis of integrin activation. Blood 102, 1155–1159.

Yang, W., Shimaoka, M., Salas, A., Takagi, J., and Springer, T.A. (2004). Intersubunit signal transmission in integrins by a receptor-like interaction with a pull spring. Proc. Natl. Acad. Sci. USA 101, 2906–2911.

Zamir, E., and Geiger, B. (2001). Components of cell-matrix adhesions. J. Cell Sci. 114, 3577–3579.